Genetic ablation of VIAAT in glycinergic neurons causes a severe respiratory phenotype and perinatal death

Jamilur Rahman · Stefanie Besser · Christian Schnell · Volker Eulenburg · Johannes Hirrlinger · Sonja M. Wojcik · Swen Hülsmann

Abstract Both glycinergic and GABAergic neurons require the vesicular inhibitory amino acid transporter (VIAAT) for synaptic vesicle filling. Presynaptic GABA concentrations are determined by the GABA-synthesizing enzymes glutamate decarboxylase (GAD)65 and GAD67, whereas the presynaptic glycine content depends on the plasma membrane glycine transporter 2 (GlyT2). Although severely impaired, glycinergic transmission is not completely absent in *GlyT2*-knockout mice, suggesting that other routes of glycine uptake or de novo synthesis of glycine exist in presynaptic terminals. To investigate the consequences of a complete loss of glycinergic transmission, we generated a mouse line with a conditional ablation of *VIAAT* in glycinergic neurons by crossing mice with loxP-flanked *VIAAT* alleles with a *GlyT2-Cre* transgenic mouse line. Interestingly, conditional *VIAAT* knockout (*VIAAT* cKO) mice were not viable at birth. In addition to the dominant respiratory failure, *VIAAT* cKO showed an umbilical hernia and a cleft palate. Immunohistochemistry revealed an almost complete depletion of VIAAT in the brainstem. Electrophysiology revealed the absence of both spontaneous glycinergic and GABAergic inhibitory postsynaptic currents from hypoglossal motoneurons. Our results demonstrate that the deletion of *VIAAT* in *GlyT2-Cre* expressing neurons also strongly affects GABAergic transmission and suggest a large overlap of the glycinergic and the GABAergic neuron population during early development in the caudal parts of the brain.

Keywords Embryonic development · Transmitter release · Vesicular filling · Electrophysiology · Brainstem

S. Hülsmann and S. M. Wojcik contributed equally.

J. Rahman · C. Schnell · S. Hülsmann
Institute for Neurophysiology and Cellular Biophysics, Georg-August-University Göttingen, Humboldtallee 23, 37073 Göttingen, Germany

S. Besser · J. Hirrlinger
Carl-Ludwig-Institute for Physiology, University of Leipzig, Liebigstrasse 27, 04103 Leipzig, Germany

C. Schnell · S. Hülsmann
Center for Nanoscale Microscopy and Molecular Physiology of the Brain (CNMPB), Göttingen, Germany

Present Address:
C. Schnell
Divisions of Pathophysiology and Repair and Neuroscience, School of Biosciences, Cardiff University, Cardiff, UK

V. Eulenburg
Institute for Biochemistry and Molecular Medicine, University of Erlangen, Fahrstrasse 17, 91054 Erlangen, Germany

J. Hirrlinger
Department of Neurogenetics, Max Planck Institute of Experimental Medicine, Hermann-Rein-Str. 3, 37075 Göttingen, Germany

S. M. Wojcik (✉)
Department of Molecular Neurobiology, Max Planck Institute of Experimental Medicine, Hermann-Rein-Straße 3, 37075 Göttingen, Germany
e-mail: wojcik@em.mpg.de

Present Address:
S. Hülsmann (✉)
Clinic for Anesthesiology, Laboratory for Experimental Neuroanesthesiology, University Hospital Göttingen, Humboldtallee 23, 37073 Göttingen, Germany
e-mail: shuelsm2@uni-goettingen.de

Introduction

Disturbances of inhibitory neurotransmission can be deleterious for the survival of mice around birth. Genetic ablation of the vesicular inhibitory amino acid transporter (VIAAT), which is also known as the vesicular GABA transporter (VGAT) results in perinatal lethality (Wojcik et al. 2006), as does the absence of Gephyrin, a postsynaptic scaffolding protein at glycinergic and GABAergic synapses (Feng et al. 1998). Other critical elements for perinatal survival are the GABA-synthesizing enzymes glutamate decarboxylase GAD65 and GAD67 (Fujii et al. 2007). On the other hand, mice lacking the glial glycine transporter 1 (GlyT1) also die shortly after birth (Gomeza et al. 2003a), whereas mice lacking the neuronal glycine transporter 2 (GlyT2) (Gomeza et al. 2003b) or the glycine receptor alpha 1 subunit (Kling et al. 1997) are initially viable but die around the second postnatal week. In contrast, knockout of genes coding for $GABA_A$ receptor subunits or plasma membrane GABA transporters (GAT) mostly does not result in early postnatal lethality. Only for the $GABA_A$ receptor γ2 subunit (Gunther et al. 1995) and the β3 subunit (Ferguson et al. 2007) neonatal lethal phenotypes with partial penetrance have been described.

Glycinergic neurotransmission has previously been tightly associated with expression of the neuronal glycine transporter GlyT2 (Zafra et al. 1995b). GlyT2 localizes to the presynaptic plasma membrane and is necessary and sufficient for achieving high glycine concentrations in the presynaptic compartment (Gomeza et al. 2003b; Aubrey et al. 2007). Interestingly, residual glycinergic neurotransmission is still observed in homozygous GlyT2 deficient mice (Gomeza et al. 2003b; Latal et al. 2010), suggesting alternative sources for the replenishment of the presynaptic glycine pool by either de novo synthesis via the mitochondrial glycine cleavage system (Davies and Johnston 1974; Kikuchi 1973) or via uptake systems of low specificity, like ASC-1 (Nakauchi et al. 2000) or the system A transporter SNAT2 (Yao et al. 2000). This residual glycinergic activity impeded the precise analysis of the impact of glycinergic neurotransmission on the function or development of neuronal networks in the CNS.

Genetic inactivation of VIAAT, which is required for vesicular uptake of glycine and GABA (McIntire et al. 1997; Sagne et al. 1997), results in an almost complete loss of GABAergic and glycinergic neurotransmission, without any induction of changes in gross brain anatomy (Saito et al. 2010; Fujii et al. 2007; Wojcik et al. 2006; Oh et al. 2010). To determine which aspects of the phenotype of *VIAAT* KO mice are caused by defects in glycinergic neurotransmission, we generated mice with a conditional inactivation of VIAAT expression specifically in glycinergic neurons. Interestingly, conditional knockout (cKO) of *VIAAT* in glycinergic neurons resulted in a phenocopy of the conventional *VIAAT* KO mice, although the loss of VIAAT expression was restricted to caudal regions of the CNS. The abolishment of both GABAergic and glycinergic synaptic inhibition suggests that almost all inhibitory neurons in caudal brain regions express the glycinergic marker protein GlyT2 at some time point during development, indicating that glycinergic neurons are capable of co-releasing GABA during early development and vice versa.

Materials and methods

Animal ethics

Animals were bred in the animal facility of the Max Planck Institute for Experimental Medicine (*VIAAT* cKO) and in the animal facility of the University medical center (GlyT2-EGFP) and treated in accordance with the German Protection of Animals Act (TierSchG Section 4 Abs. 3) and with the guidelines for the welfare of experimental animals issued by the European Communities Council Directive, November 24th, 1986 (86/609/EEC). The experiments were communicated to and notified by the animal welfare office of University Medical Center Göttingen (institutional act number T12/11).

Generation of conditional *VIAAT* knockout mice

Conditional *VIAAT* knockout mice ($VIAAT^{fl/fl}$) were generated through homologous recombination in embryonic stem (ES) cells (129/ola) (Fig. 1). The targeting vector was based on a genomic 11.2 kb BamHI-SbfI fragment subcloned from a Lambda FIXII 129/Sv phage library (Stratagene) and also included two thymidine kinase cassettes for negative selection. The neomycin cassette (neo) for positive selection and the loxP sites for Cre-mediated excision were introduced into the targeting vector by homologous recombination in *E. coli* (Liu et al. 2003). Bacterial strains and plasmids for the bacterial recombineering steps were obtained from the National Cancer Institute at Frederick (http://ncifrederick.cancer.gov/research/brb). The neomycin (neo) cassette, which was flanked by two recognition sites for Flp-recombinase, was removed from the targeted *VIAAT* allele ($VIAAT^{neo-fl}$) by breeding chimeric B6.129ola-$VIAAT^{neo-fl}$ males to a Flp-deleter strain (JAX® strain 016226, B6 N.129S4-$Gt(ROSA)26Sor^{tm1(FLP1)Dym}$). Mice homozygous for the conditional *VIAAT* allele ($VIAAT^{fl/fl}$) were indistinguishable from wild-type (WT) littermates. Successful inactivation of the *VIAAT* gene in response to Cre-mediated recombination was initially confirmed in vitro by lentiviral expression of Cre in cultured striatal neurons from postnatal day 0

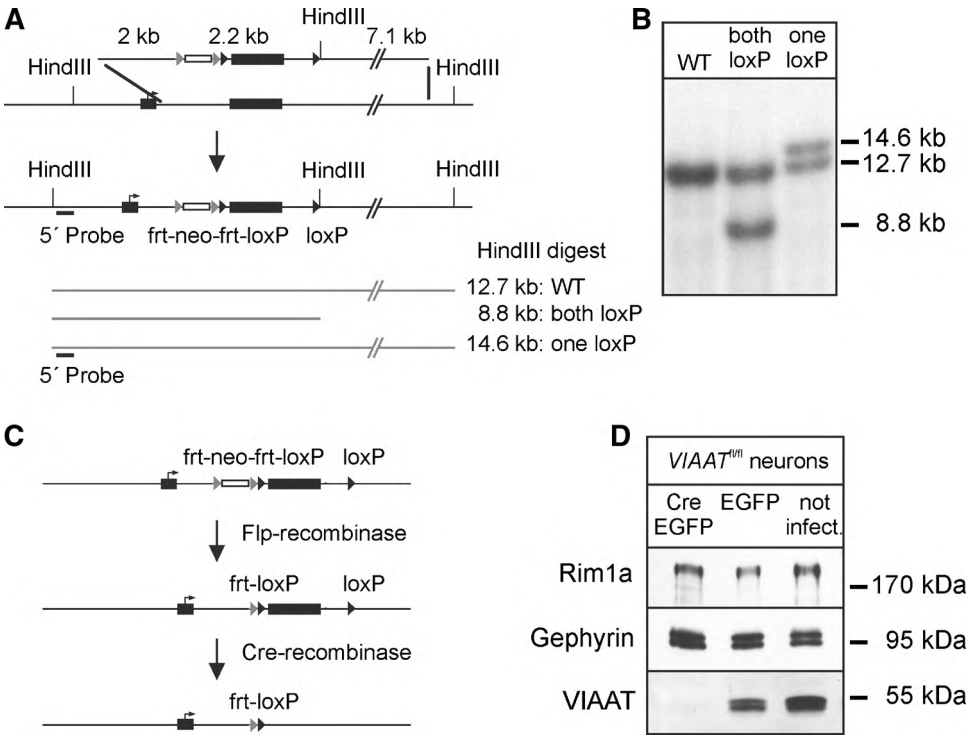

Fig. 1 Targeting strategy for generating the *VIAAT*$^{fl/fl}$ mice. **a** A targeting vector was used to introduce two recognition sites (loxP) for Cre, one directly upstream of the second exon and one downstream of the 3′ untranslated region of the *VIAAT* gene. The *arrow* in the first exon indicates the position of the start codon. The vector contained a neomycin resistance cassette (neo) for positive selection, flanked by two recognition sites (frt) for Flp-recombinase. A HindIII restriction site was introduced to aid detection of the integration of the distal loxP site. The 5′ probe used for Southern analysis of targeted ES-cell clones should result in a 12.7 kb HindIII fragment for WT, 8.8 kb for the integration of both loxP sites and a 14.6 kb fragment for the integration of only the proximal loxP site. **b** Southern blot of HindIII digested clonal ES-cell DNA. Clones containing the desired integration of both loxP sites (8.8 and 12.7 kb bands) were selected for further analysis and blastocyst injection. **c** Mice carrying the targeted allele containing the neo cassette were bred to mice expressing Flp-recombinase to remove the neo cassette. Expression of Cre results in the deletion of the second *VIAAT* exon, as well as the 3′ untranslated region. **d** To confirm the inactivation of the *VIAAT* gene upon Cre-mediated recombination, striatal neurons were cultured from *VIAAT*$^{fl/fl}$ pups on postnatal day 0. On day in vitro (DIV) 1, the cultures were then infected with a lentivirus expressing Cre and EGFP. Uninfected cultures and cultures infected with a lentivirus expressing only EGFP were used as controls. At DIV12, no VIAAT protein was detectable by Western blotting in Cre-infected cultures. An antibody recognizing Gephyrin, a postsynaptic marker of inhibitory synapses and an antibody to the presynaptic protein Rim1α were used as controls

VIAAT$^{fl/fl}$ pups (Fig. 1d). Antibodies used for Western blotting were: rabbit anti-VIAAT at 1:1,000, and mouse anti-Gephyrin 3B11 at 1:20,000 (both from Synaptic Systems) and mouse anti-Rim at 1:500 (Transduction Laboratories).

To achieve a cell type specific deletion of the *VIAAT* gene in glycinergic neurons, *VIAAT*$^{fl/fl}$ mice were crossbred with mice expressing Cre recombinase (Cre) under the control of a BAC transgenic *GlyT2* promoter fragment (*GlyT2-Cre*; official strain name Tg(Slc6a5-iCre)^{121Veul}). Animals used in experiments were from timed matings of *GlyT2-Cre*, *VIAAT*$^{fl/wt}$ males with homozygous *VIAAT*$^{fl/fl}$ or heterozygous *VIAAT*$^{fl/wt}$ females. Offspring from these matings with the following genotypes were used as control (Ctrl): all *GlyT2-Cre* negative mice and those *GlyT2-Cre* positive animals without the conditional *VIAAT* allele (*Glyt2-Cre*, *VIAAT*$^{wt/wt}$). Heterozygous mice (Het) were *GlyT2-Cre* positive and heterozygous for the conditional *VIAAT* allele (*GlyT2-Cre*, *VIAAT*$^{fl/wt}$). Throughout the manuscript we refer to *Glyt2-Cre*, *VIAAT*$^{fl/fl}$ animals, in which the *VIAAT* gene is deleted in *GlyT2-Cre* expressing neurons, as conditional knockout (cKO) mice. The day of vaginal plug detection was defined as embryonic state (E) 0.5.

Cesarean section

Pregnant female mice were killed by cervical dislocation under deep isoflurane anesthesia. Embryos were quickly removed from the uterus and immediately cleaned with lab wipes and were then placed under an infrared lamp to prevent cooling. Images of embryos were taken with a Canon EOS 400 digital camera (Canon, Krefeld, Germany). Whole embryo paraffin sections were stained with

hematoxylin and eosin and images were taken using a Leica MZ16 F stereomicroscope mounted with a Leica DFC350 FX camera (Leica Camera AG, Solms, Germany).

Whole-body plethysmography and lung buoyancy test

Breathing was measured by whole-body plethysmography that records pressure changes resulting from the warming of the inspired air and cooling during expiration (Drorbaugh and Fenn 1955). The embryos were placed in a 30 ml chamber that was connected to a differential low-pressure transducer (model DP1 03, Validyne Engineering, Northridge, CA). The signal from the pressure transducer that was captured by a sine wave carrier demodulator (CD-15, Validyne Engineering) was digitized (1 kHz sampling rate) with an analog–digital interface (PowerLab/4 s) and Chart-Software (ADInstruments GmbH, Spechbach, Germany). Pressure traces were converted to axon binary format and analyzed by the threshold based event detection method using clampfit software (Molecular Devices, Sunnyvale, CA). Embryos remained in the chamber for 2 min and periods (60 s), lacking movement artifacts, were identified and analyzed offline. The respiratory frequency was calculated as the reciprocal of the averaged inspiratory interval. For the lung buoyancy (floating) test, lungs were placed in phosphate buffer saline after removal from the thorax.

Preparation of brain slices

Electrophysiological experiments were performed on medullary slice preparations from E 18.5 embryos. Embryos were decapitated and the brain was quickly isolated from the skull. Brainstems were dissected from the forebrain and placed in carbogen-saturated (95 % O_2, 5 % CO_2) ice-cold artificial cerebrospinal fluid (ACSF) that contained 118 mM NaCl, 3 mM KCl, 1.5 mM $CaCl_2$, 1 mM $MgCl_2$, 1 mM NaH_2PO_4, 25 mM $NaHCO_3$, and 30 mM D-glucose. The osmolarity was approximately 310 mosm/l and pH was adjusted to 7.4 using 1 N NaOH. Transverse slices were cut with a vibratome (VT1200S, Leica, Bensheim, Germany) in a rostro-caudal-direction using various steps until the lower brainstem was reached and the principal nucleus of inferior olive became visible. For recordings from hypoglossal motoneurons, 250–280 µm slices were cut as described before (Latal et al. 2010). Slices were stored in ACSF at room temperature for at least 30 min before starting an experiment. Subsequently they were transferred to a recording chamber and kept submerged by a grid of nylon fibers for mechanical stabilization. The chamber was mounted on a Zeiss Axioscope microscope (Zeiss, Germany) and continuously perfused with ACSF (room temperature; 20–23 °C) at a flow rate of 4–7 ml/min. For analysis of respiratory network function, 600–650 µm thick slices were prepared as described earlier (Winter et al. 2009; Rahman et al. 2013), exposing the principal nucleus of the inferior olive and the preBötzinger complex (preBötC) at the upper surface. These slices were continuously superfused with 8 mM K^+-containing ACSF at 30 °C to secure long-term rhythmic activity that could be recorded via field potential electrodes.

Electrophysiological recordings

Whole-cell recordings were obtained with Multiclamp 700B patch-clamp amplifier (Molecular Devices, LLC, Sunnyvale, CA, USA). Recording electrodes were pulled from borosilicate glass capillaries (Biomedical Instruments, Zöllnitz, Germany) on a horizontal pipette-puller (Zeitz, Munich, Germany). Resistance of electrodes ranged from 3 to 6 MΩ using an intracellular solution containing (in mM) 140 KCl, 1 $CaCl_2$, 2 $MgCl_2$, 4 Na_2ATP, 10 HEPES, 10 EGTA (pH 7.2; adjusted with KOH). Hypoglossal motoneurons were identified by their location and size (Hulsmann et al. 2000) and voltage-clamped at a holding potential of −70 mV. With a chloride equilibrium potential $E^-_{[Cl]}$ at 0 mV, inhibitory postsynaptic currents (IPSCs) were recorded as inward currents. Synaptic currents were filtered at 3 kHz. Further noise reduction was achieved by electrically filtering the signals with a humbug-noise eliminator (Quest Scientific, North Vancouver, Canada). Signals were digitized at 10 kHz using DigiData 1440 interface and pClamp software (Molecular Devices) and stored on hard disk for offline analysis.

Spontaneous inhibitory postsynaptic currents (sIPSCs) were recorded in ACSF containing 20 µM 6-cyano-7-nitroquinoxaline-2,3-dione (CNQX) and 100 µM DL-2-amino-5-phosphonopentanoate (AP5). Extracellular recording of the preBötC activity was performed with 1 MΩ glass microelectrodes filled with ACSF. Field potentials were amplified by a custom-built AC-amplifier (5,000×), band-pass-filtered (0.25–1.5 kHz), rectified and integrated (Paynter filter). Recordings were digitized at 1 kHz and stored using a miniDigi 1B interface and pClamp (Molecular Devices, LLC, Sunnyvale, CA, USA).

To elicit postsynaptic glycinergic or GABAergic currents, glycine (1 mM) or GABA (10 mM) was applied from a patch electrode using a pressure ejection system (NPI-electronic, Tamm, Germany) that was controlled by Clampex software. Patch electrode for drug application had a resistance of 2–4 MΩ and was placed in a distance of 20–30 µm from the recorded motoneurons. The pressure was set to 1 kPa and the neurotransmitter was applied for 20 ms (30 s intervals). The amplitude of four subsequent evoked (e) IPSCs was averaged and used for further analysis.

Immunofluorescence analysis

For immunofluorescence analysis, brains were isolated as described above and immediately stored in 4 % paraformaldehyde in phosphate-buffered saline (PBS) containing (in mM) NaCl 137, KCl 2.7, Na_2HPO_4 8.1, KH_2PO_4 1.4 as described before (Winter et al. 2007). After 24 h, brains were rinsed in PBS and the brainstem was isolated. Transverse slices (40 µm) were cut using a vibratome (VT1200S, Leica, Bensheim, Germany). Before staining, slices were washed with PBS (four times 5 min). For VIAAT-staining, slices were permeabilized in blocking buffer (10 % normal donkey serum, 5 % sucrose, 0.4 % Triton X-100, 0.2 % NaN_3 in 1 × PBS) for 1 h at room temperature. The blocking buffer was replaced with staining buffer (2 % normal donkey serum, 5 % sucrose, 0.4 % Triton X-100, 0.2 % NaN_3 in 1× PBS) containing rabbit anti-VIAAT (1:800; Cat no. 131-003; Synaptic System, Göttingen) and incubated at 4 °C for 72 h. After rinsing in PBS, the secondary Cy3-Donkey-Anti-rabbit-IgG (1:1,000; Cat. No. AP182C; Merck Millipore, USA) was applied for 2 h at room temperature in the dark to avoid bleaching of fluorescent dye. For choline acetyltransferase (ChAT)-staining, slices were permeabilized in 0.4 % Triton in PBS for 30 min, and non-specific antibody binding was minimized by adding 4 % normal donkey serum in PBS with 0.2 % Triton. Sections were incubated with the primary anti-ChAT-antibody (Chemicon, Temecula, CA, USA) overnight in 1 % serum in PBS with 0.05 % Triton (4 °C) and labeled with Cy5-/Alexa647-conjugated secondary antibodies the following day (room temperature, 2 h, anti-goat from donkey, 1:250 dilution; Jackson IR, Newmarket, UK). After a final washing step, slices were transferred onto microscopic slides (Thermo Fischer Scientific, Germany) and allowed to dry for minimum 30 min in darkness before mounting in Fluorescent Mounting Medium (Dako Industries, Carpinteria, CA). Negative controls were conducted by omitting the primary antibody from the protocol described above. Fluorescence microscopy was performed on a confocal laser scanning microscope (LSM 510 Meta, Zeiss, Oberkochen, Germany). Cy3 was excited at 546 nm. Fluorescence was detected through a 560–600 nm band-pass filter. Cy5-fluorescence was visualized at 633 nm excitation through a 650-nm-long pass filter.

Analysis of VIAAT expression was performed in regions of interest (ROI) that were matched to the size of the analyzed brain region using the Atlas of the developing mouse brain for reference (Paxinos 2007). ROI size was 173 × 181 µm for hypoglossal nucleus ($N = 6$ embryos), 100 × 100 µm for the preBötC ($N = 3$) and 237 × 237 µm for the ventromedial hypothalamus ($N = 4$). All parameters (objective, laser intensity, pinhole, offset, gains, ROI size) were identical for cKOs and Ctrls. VIAAT-immunoreactivity was quantified by defining the area fraction of VIAAT positive pixel (puncta) using the "Analyze particle" tool of the analysis software ImageJ (http://rsb.info.nih.gov/ij/). Only pixels above a threshold (that was defined by the mean of the maximal intensity of at least two independent negative control stainings; Histogram tool; ImageJ) were defined as VIAAT puncta. Finally the area fraction was calculated as VIAAT puncta/total pixels in ROI (in %).

For GABA staining, TgN(Slc6a5-EGFP)1Uze embryos and pups were decapitated, the brains removed from the skull and fixed in 4 % PFA/PBS for 24 h. Free-floating coronal sections of the brainstem were stabilized in PBS. Sections were incubated overnight at 4 °C with the primary antibody (rabbit anti-GABA, 1:5,000, Sigma, Cat. No. A2052) diluted in blocking reagent (2 % normal goat serum in PBS). Sections were washed three times for 10 min in PBS and incubated for 2 h at room temperature with the secondary antibody goat anti-rabbit Cy3 (Dianova/Jackson Immuno Research, Cat. No. 111-165-144). After washing with PBS, sections were incubated in PBS containing the nuclear marker DAPI (Roth, Cat. No. 6335.1) for 5 min and finally mounted in Immu-Mount (Thermo Scientific, Cat. No. 9990402). Confocal Images were acquired using a Zeiss LSM700 Axio Observer laser scanning microscope. EGFP was excited at 488 nm. Fluorescence was detected through a 555 nm short pass filter. Red fluorescence was visualized at 546 nm excitation through a 560-nm-long pass filter.

Quantification of GABAergic cells was performed on $N = 3$ animals, for each of which cells were counted in three 45-µm-thick sections per animal and three areas per section in a 320 × 320 µm frame using ImageJ. The three areas analyzed in each slice were always selected in the same orientation toward the nucleus ambiguous in all slices of all mice. The number of cells double positive for GABA and GlyT2 was determined in the same depth within all slices (between 5 and 7 µm below the surface) using z-stack recordings (total z-size 10–15 µm) to ensure identical permeation conditions for the antibodies.

Electrocardiography (ECG)

Electrocardiography was recorded immediately after removal of the embryos from the mother. Bipolar ECG recordings were conducted between the forelimbs of the embryo by wiring of the mice to the field potential amplifier using small stainless steel clips. For a reference, a third clip was placed at the tail or a hind limb. Recordings were conducted for 1 min to keep the skin irritation to a minimum. The signal was amplified 1,000×, filtered (low pass 500 Hz), digitized at 10 kHz using DigiData 1440

Table 1 Distribution of genotypes

Parents	Embryos No.	Ctrl *VIAAT*$^{wt/wt}$, *GlyT2* Cre−	Ctrl *VIAAT*$^{fl/wt}$, *GlyT2* Cre−	Ctrl *VIAAT*$^{fl/fl}$, *GlyT2* Cre−	Ctrl *VIAAT*$^{wt/wt}$, *GlyT2* Cre+	Het *VIAAT*$^{fl/wt}$, *GlyT2* Cre+	cKO *VIAAT*$^{fl/fl}$, *GlyT2* Cre+
VIAAT$^{fl/fl}$, *GlyT2* Cre− × *VIAAT*$^{fl/wt}$, *GlyT2* Cre+	126	0 [0 (0 %)]	37 [31.5 (25 %)]	25 [31.5 (25 %)]	0 [0 (0 %)]	28 [31.5 (25 %)]	36 [31.5 (25 %)]
VIAAT$^{fl/wt}$, *GlyT2* Cre− × *VIAAT*$^{fl/wt}$, *GlyT2* Cre+	243	31 [30.4 (12.5 %)]	64 [60.8 (25 %)]	28 [30.4 (12.5 %)]	35 [30.4 (12.5 %)]	55 [60.8 (25 %)]	30 [30.4 (12.5 %)]
Total	369	31 [30.4]	101 [92.3]	53 [61.9]	35 [30.4]	83 [92.3]	66 [61.9]

Embryos were derived from two different breeding paradigms using either mice homozygous for the conditional *VIAAT* allele and negative for the Cre recombinase (*VIAAT*$^{fl/fl}$, *GlyT2 Cre*−) or heterozygous for the conditional *VIAAT* allele and negative for the Cre recombinase (*VIAAT*$^{fl/wt}$, *GlyT2 Cre*−) for timed matings with Cre positive mice that are heterozygous for the conditional *VIAAT* allele (*VIAAT*$^{fl/wt}$, *GlyT2 Cre*+). The numbers represent the actual numbers of genotyped embryos obtained by caesarian section. In brackets expected numbers of animals are given (the expected percentage of embryos follows in parenthesis)

interface and pClamp software (Molecular Devices) and stored on hard disk for offline analysis. Heart rate was calculated as the mean of the reciprocal of RR-interval of 10 successive QRS-complexes.

Data handling and statistics

Electrophysiological data were stored on hard disk of a personal computer for offline analysis. IPSC amplitude and frequency were analyzed using the MiniAnalysis program (Jaejin Software, Leonia, NJ) as described earlier (Latal et al. 2010). For data analysis Microsoft Excel (Redmond, WA) and SigmaPlot (Systat Software, San Jose, CA) was used. Results are expressed as mean ± standard error (SE). For statistical analysis *t* tests or Mann–Whitney Rank Sum tests were used and differences were considered significant if $p < 0.05$. Mendelian distribution of embryos was tested using Chi square test.

Results

Appearance and breathing of *VIAAT* cKO embryos

Live *VIAAT* cKO (*GlyT2-Cre*, *VIAAT*$^{fl/fl}$) pups were never found in any litter. Therefore, we delivered embryos at E18.5 by caesarian section (CS). A total of 369 embryos were genotyped after CS, revealing 66 *VIAAT* cKO embryos (Table 1). These numbers matched the expected ratio, suggesting a normal Mendelian distribution at E18.5 (Chi square test; $p = 0.546$). Therefore, losses during earlier developmental stages are unlikely.

VIAAT cKO embryos could be easily identified by their gross anatomical appearance (Fig. 2). While Ctrl embryos (*GlyT2-Cre*, *VIAAT*$^{wt/wt}$ and all embryos without *GlyT2-Cre*) and embryos heterozygous (Het) for the targeted *VIAAT* allele (*GlyT2-Cre*, *VIAAT*$^{fl/wt}$) had a normal muscle tone and responded to handling with body movements, *VIAAT* cKO mice (*GlyT2-Cre*, *VIAAT*$^{fl/fl}$) were not moving and exhibited a hunched (kyphotic) posture (Fig. 2b). Noteworthy, *VIAAT* cKO mice showed a defect of the ventral body wall that is best described as a persistent umbilical hernia or omphalocele ($n = 54$; Fig. 2). Furthermore, *VIAAT* cKO mice also showed a defective developmental closure of the palate (Fig. 2d). Thus, the *GlyT2-Cre* driven *VIAAT* cKO closely resembles the gross phenotype of *VIAAT* KO mice with a global deletion of the *VIAAT* gene (Wojcik et al. 2006).

The skin color of Ctrl and *VIAAT* cKO mice was very similar during CS and immediately after the removal from the uterus but cKO mice quickly turned cyanotic. Moreover, we could not detect any breathing by plethysmography in *VIAAT* cKOs ($n = 9$), while all Het mice ($n = 6$)

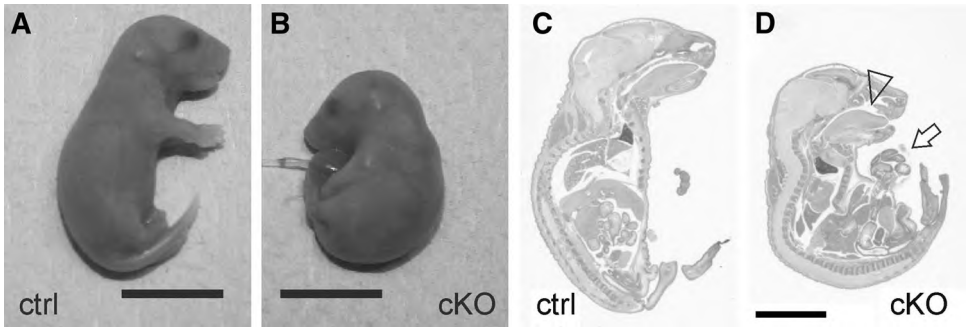

Fig. 2 Multiple phenotypic changes in *VIAAT* cKO mice. **a**, **b** Ctrl mice delivered by CS at E18.5 acquire pink skin quickly and show spontaneous limb movements. *VIAAT* cKO littermates, although pink when the umbilical cord is intact, turn cyanotic after removal from the mother. **c** Sagittal hematoxylin and eosin stained whole embryo section of WT embryo compared to **d** cKO embryo, which shows an umbilical hernia (omphalocele; *arrow*) and a cleft palate (*arrow head*). *Scale bar* in **a**, **b** = 10 mm, *Scale bar* in **c**, **d** = 5 mm

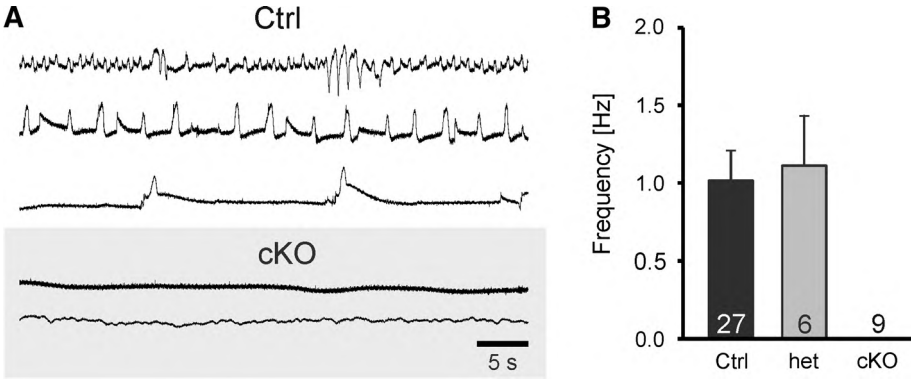

Fig. 3 *VIAAT* cKO mice do not breathe. **a**, **b** Plethysmography reveals apnea in the *VIAAT* cKOs. While Ctrl mice quickly started to breathe, no air movement was detected in cKO mice (basic statistics shown in (**b**); see also Table 1). Notably, the initial breathing rate of Ctrl mice is very variable

Table 2 Frequency of different phenotypes

	Omphalocele	Cleft palate	Breathing in plethysmography	Positive lung floating test
Ctrl	0/177	0/76	22/27	7/7
cKO	54/54	23/23	0/9	0/9

Comparison of the frequency of the phenotypes (omphalocele) or umbilical hernia, cleft palate, breathing detected in plethysmography and positive lung floating test of embryos with a conditional *VIAAT* knockout (cKO) in glycinergic neurons, and the Ctrl littermates expressed as the number embryos exhibiting a particular phenotype over the total number examined for that phenotype

and 22 of 27 Ctrl littermates started to breathe and gained a nice pink skin color (Fig. 3a; Table 2). The breathing frequencies of the WT (1.0 ± 0.19 Hz) and Het mice were (1.1 ± 0.3 Hz) indistinguishable (Fig. 3b). Since whole-body plethysmography, however, cannot exclude that *VIAAT* cKOs take an initial breath between CS and placement in the plethysmography chamber, we also isolated lungs from the thorax of Ctrl and cKO embryos and performed a lung floating (buoyancy) test. While Ctrl/WT lungs floated on the surface ($n = 7$), cKO lungs sank to the bottom ($n = 9$) indicating that cKO embryos never take a breath (Table 2).

Dramatic reduction of VIAAT immunoreactivity in the hypoglossal nucleus and ventrolateral medulla, but not in the hypothalamus of *VIAAT* cKO embryos

To assess the extent of VIAAT deletion in cKO mice we first performed an immunohistochemical analysis in different brain regions. In caudal brain regions that are known to have high levels of GlyT2 (Luque et al. 1995; Jursky and Nelson 1996), we observed a strong reduction of VIAAT expression in the cKO mice. In the hypoglossal nucleus of cKO mice, the VIAAT puncta area fraction was reduced to 5 % of Ctrl animals (Ctrl 81.48 ± 2.00 %; cKO 4.35 ± 1.10 %; $p < 0.05$; $n = 6$; Fig. 4). A similar reduction was observed in the ventrolateral medulla and in the preBötC (Ctrl 75.72 ± 8.32 % vs. KO 6.35 ± 2.05 %; $p < 0.05$; $n = 3$; Fig. 5a–d), suggesting a general elimination of VIAAT expression in brain regions with high numbers of glycinergic neurons.

In contrast, VIAAT expression in cKO embryos was not reduced in the ventromedial hypothalamus (area fraction = 82.47 ± 4.04 % (Ctrl) vs. 83.47 ± 2.71 % (KO; n.s; Fig. 5e–h), a brain region that has few glycinergic neurons and is only a minor target of glycinergic projections, but has significant GABAergic transmission (Zafra et al. 1995b;

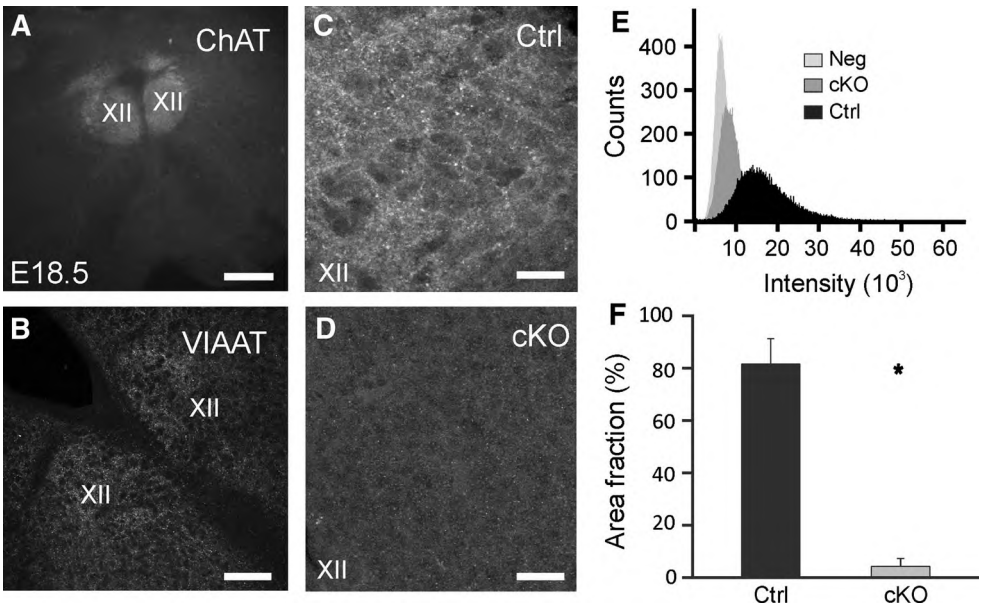

Fig. 4 Immunofluorescence analysis reveals abolished VIAAT expression in the hypoglossal nucleus of *VIAAT* cKO embryos. **a** Hypoglossal nucleus (XII) in the E18.5 embryo was identified by anti-ChAT-immunostaining. **b** Overview of the VIAAT expression in the hypoglossal nucleus of a Ctrl embryo; Primary Antibody: rabbit anti-VIAAT (Synaptic Systems), secondary antibody: Cy3-conjugated-anti-rabbit-IgG. **c** VIAAT immunostaining in the hypoglossal nucleus from a Ctrl embryo. **d** In cKO embryos, VIAAT immunostaining is almost absent. **e** Fluorescence intensity histogram from the hypoglossal nucleus of negative control (Neg, no primary antibody), cKO embryo, and Ctrl embryo. **f** The average pixel area fraction (Image J) of VIAAT-(Cy3)-fluorescence from cKO embryos is significantly smaller as compared to Ctrl embryos. *Scale bars* **a** 300 μm, **b** 100 μm, and **c**, **d** 30 μm

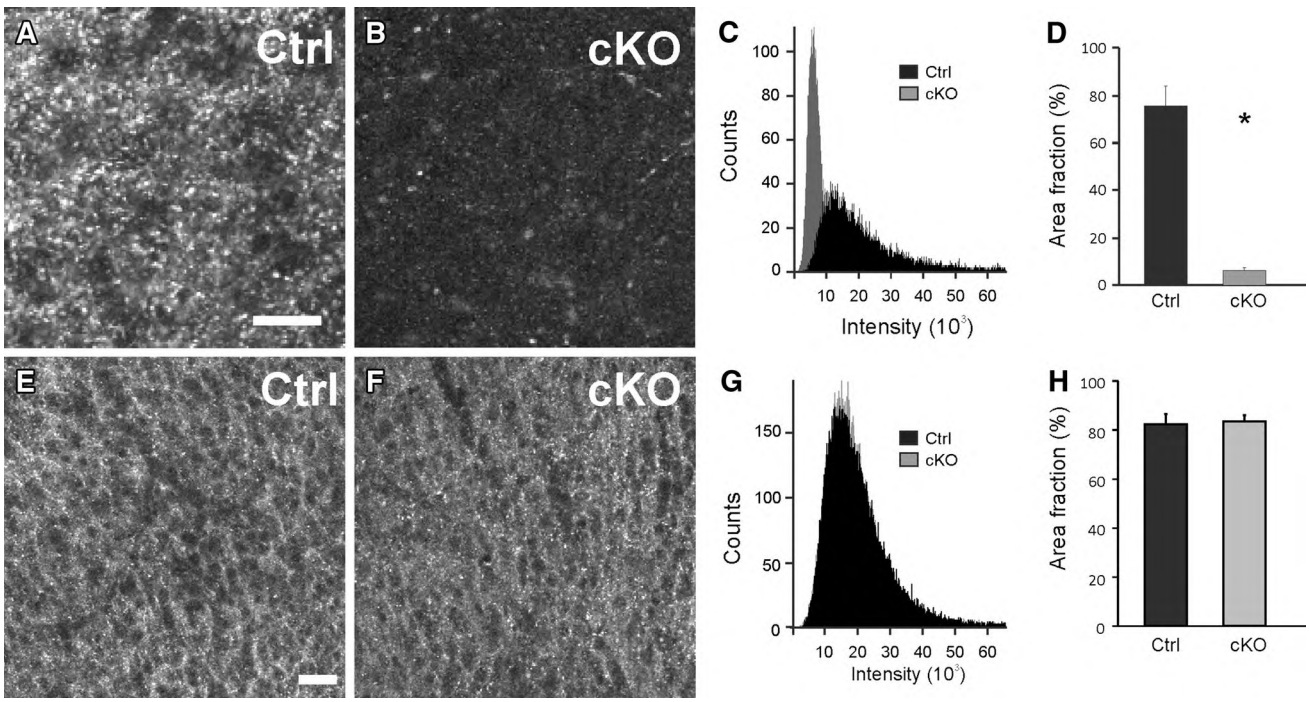

Fig. 5 VIAAT is not reduced in ventromedial hypothalamus of *VIAAT* cKO embryos. **a**, **b** VIAAT-staining in the preBötC from Ctrl embryo (**a**, Ctrl) and cKO embryo (**b**, KO). **c** Intensity histogram from preBötC from Ctrl and cKO embryos. **d** The pixel area fraction is reduced to a minimum in VIAAT cKO mice. **e** VIAAT-staining in the hypothalamus from Ctrl embryo; **f** VIAAT-staining from hypothalamus of cKO embryo with similar intensity. **g** Intensity histogram from hypothalamus from cKO and Ctrl embryos. **h** The pixel area fraction does not differ between *VIAAT* cKO and Ctrl littermates. *Scale bars* 20 μm

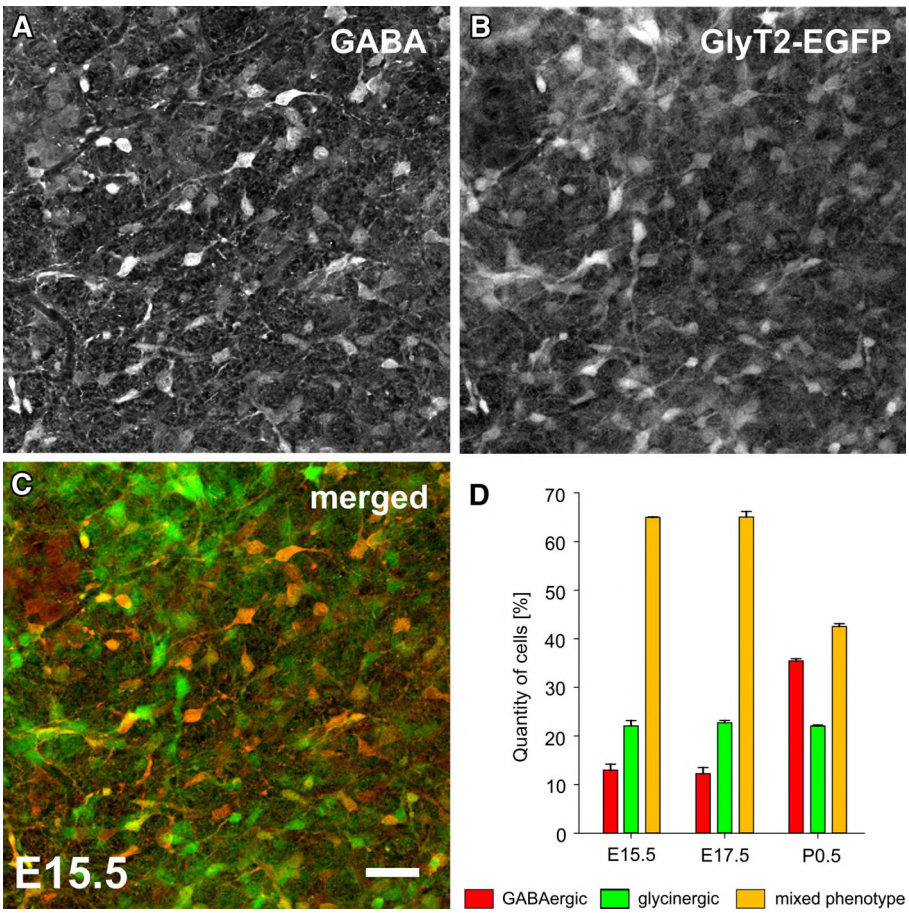

Fig. 6 Distribution of GABAergic and glycinergic neurons in the embryonic medulla. Immunohistochemical identification of GABAergic neurons (**a**) in the ventrolateral medulla of TgN(GlyT2-EGFP; **b**) mice that use the same promoter sequence as the *GlyT2-Cre* mice at embryonic day (E)15.5. The staining for GABAergic neurons was performed with an antibody raised against PFA-fixed GABA; secondary antibody Cy3. **c** The merged image shows the high degree of colocalization of GABA-immunoreactivity with glycinergic cells (*green*); *scale bar* 40 µm. **d** Quantification of the different inhibitory phenotypes during embryonic development

Jursky and Nelson 1995; Zeilhofer et al. 2005; Jo 2012), indicating that the conditional deletion of the *VIAAT* gene is limited to caudal brain regions with high GlyT2 expression.

Predominance of the mixed GABAergic/glycinergic phenotype in the ventrolateral medulla during embryonic development

The strong reduction of VIAAT expression in caudal parts of the brain is in line with the assumption that during embryonic development most inhibitory neurons in this brain region express GlyT2. In *VIAAT* cKO embryos, the *GlyT2-Cre* driven DNA recombination leading to the inactivation of the *VIAAT* gene takes place at a point in embryonic development before the respiratory network becomes active (Thoby-Brisson et al. 2009). To assess the degree of *GlyT2*-promoter activity in GABA-positive neurons at this early developmental stage, we quantified the degree of overlap between EGFP expression and GABA-immunoreactivity in transgenic mice expressing EGFP under the control of the *GlyT2*-promoter (Zeilhofer et al. 2005). We consistently found that only a minor fraction of inhibitory neurons was labeled only for GABA (13.0 ± 1.2 % at E15.5 and 12.3 ± 1.2 % at E17.5), while the remaining 87 % where either "yellow" and thus had a mixed GABAergic/glycinergic phenotype (65.0 ± 0.1 % at E15.5; 65 ± 1.1 % at E17.5) or "green", i.e. had a pure glycinergic phenotype (22.1 ± 1.1 % at E15.5; 22.7 ± 0.5 % at E17.5; Fig. 6). In comparison, after birth (P0.5) the fraction of pure GABAergic neurons increased to 35.5 ± 0.5 % ($p < 0.05$) at the expense of cotransmitting cells ($p < 0.05$) while the percentage of pure glycinergic neurons remained stable 22.0 ± 0.2 %.

Lack of inhibitory synaptic transmission in *VIAAT* cKO mice

The reduction of VIAAT expression in the brainstem of *VIAAT cKO mice* was almost complete, suggesting that in almost all inhibitory neurons within this brain region, Cre-mediated recombination had occurred. To test this on a functional level, we recorded spontaneous inhibitory postsynaptic currents (sIPCS) from hypoglossal motoneurons. These neurons have been proven to be an invaluable tool for the analysis of genetic defects in glycinergic synaptic transmission (Gomeza et al. 2003a, b; Latal et al. 2010). In these recordings, we failed to observe any sIPSCs

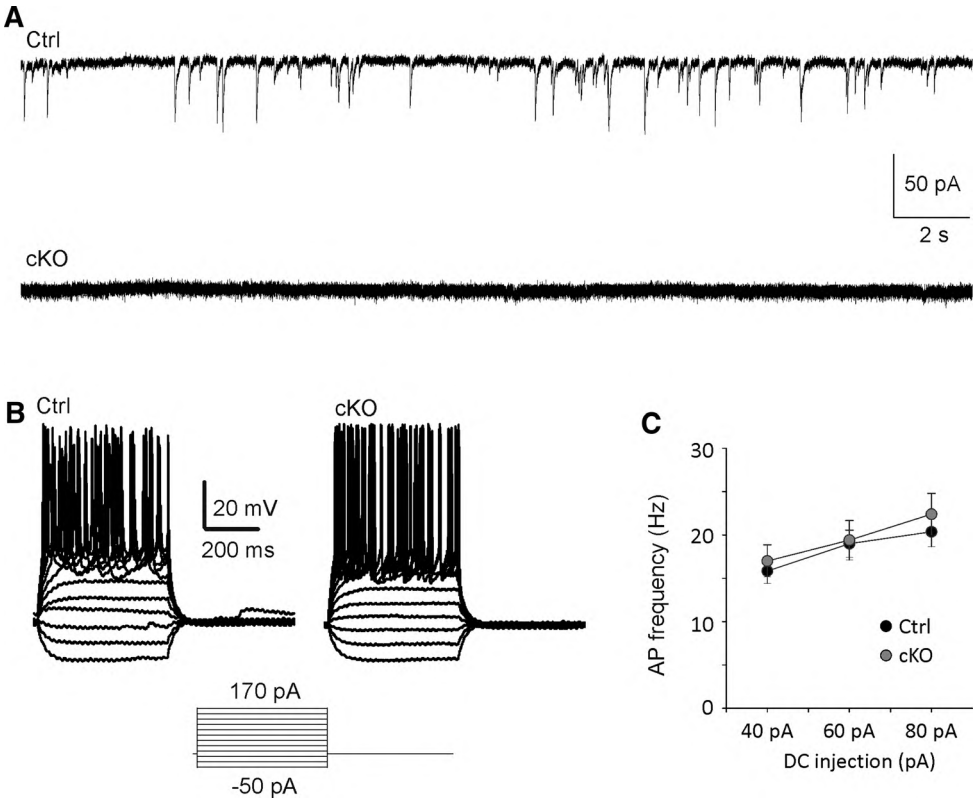

Fig. 7 Absence of IPSCs from hypoglossal neurons from *VIAAT* cKO embryos. **a** Inhibitory transmission to hypoglossal neurons in Ctrl (*upper trace*) and *VIAAT* cKO embryos (*lower trace*). Spontaneous inhibitory postsynaptic currents (sIPSCs) from Ctrl mice *VIAAT* cKO mice recorded from hypoglossal neurons in the presence of CNQX, DL-AP5, Zolpidem. **b** Membrane potential traces from a hypoglossal neuron of both Ctrl and cKO embryos in response to a DC injection (see step protocol below). **c** AP–frequency–DC current relation for cKO and Ctrl embryos

(glycinergic or GABAergic) in slices from *VIAAT* cKO mice (Fig. 7a). These data suggest that synaptic inhibition is virtually abolished in the hypoglossal nucleus.

To exclude the possibility that the failure to detect any inhibitory input to the hypoglossal motoneurons is a result of major alterations in the properties of these cells, we determined their basic electrophysiological parameters. The input resistances of Ctrl and *VIAAT* cKO N. XII-motoneurons were indistinguishable (Ctrl = 0.34 ± 0.05 GΩ; cKO = 0.42 ± 0.06 GΩ; n.s.), excluding major changes in membrane composition. Membrane capacitance of the cKO neurons was slightly but significantly smaller (44.55 ± 3.22 pF; $n = 21$) as compared to neurons from Ctrl littermates (54.87 ± 3.73 pF, $n = 28$; $p < 0.05$) and the resting membrane potential of cKO neurons (−57.57 ± 1.98 mV; $n = 35$) was more depolarized as compared to Ctrl hypoglossal motoneurons (−64.34 ± 1.28 mV; $n = 41$; $p < 0.05$). Depolarization of hypoglossal motoneurons by positive currents injections resulted in slightly higher AP frequencies in *VIAAT* cKO neurons compared to Ctrl preparations, however, this difference did not reach significance (Fig. 7b, c).

To test whether the failure of inhibitory transmission also involves changes of the postsynaptic receptor expression, we locally applied GABA or glycine to hypoglossal motoneurons. The GABA-induced current (eIPSC) was not changed in *VIAAT* cKO XII-motoneurons (Fig. 8a–c). Application of 10 mM GABA resulted in an inward current of 2.55 ± 0.97 nA ($n = 7$) in Ctrl animals and of 3.17 ± 1.15 nA in cKOs ($n = 7$; n.s.; Fig. 8b). The amplitude of the postsynaptic glycinergic currents in cKO mice (3.61 ± 0.64 nA; $n = 8$) was smaller as compared to Ctrl mice (5.28 ± 0.39 nA; $n = 6$; $p < 0.05$; Fig. 8d, e). However, when calculating the current density for glycinergic eIPSC no significant difference was detectable (Fig. 8f) suggesting that the small overall current does not result from an altered postsynaptic expression of the receptors but rather reflects the lower capacitance of the cell.

PreBötC network activity is altered in conditional *VIAAT* KO mice

To assess the respiratory network function in the *VIAAT* cKO mice, we analyzed respiratory rhythmic slice preparations cut from the level of the preBötC of E18.5 embryos (Winter et al. 2007, 2009; Gomeza et al. 2003a). PreBötC network activity was detectable in all tested WT embryos ($n = 6$). The activity was irregular; however, this is typical for newborn mice (Gomeza et al. 2003a). We also found bursting activity in the preBötC in 4 out of 6 slices from *VIAAT* cKO mice. Since it has been shown that at birth, chloride-mediated transmission is inhibitory (Tyzio et al. 2006; Gomeza et al. 2003a), we tested if blockade of

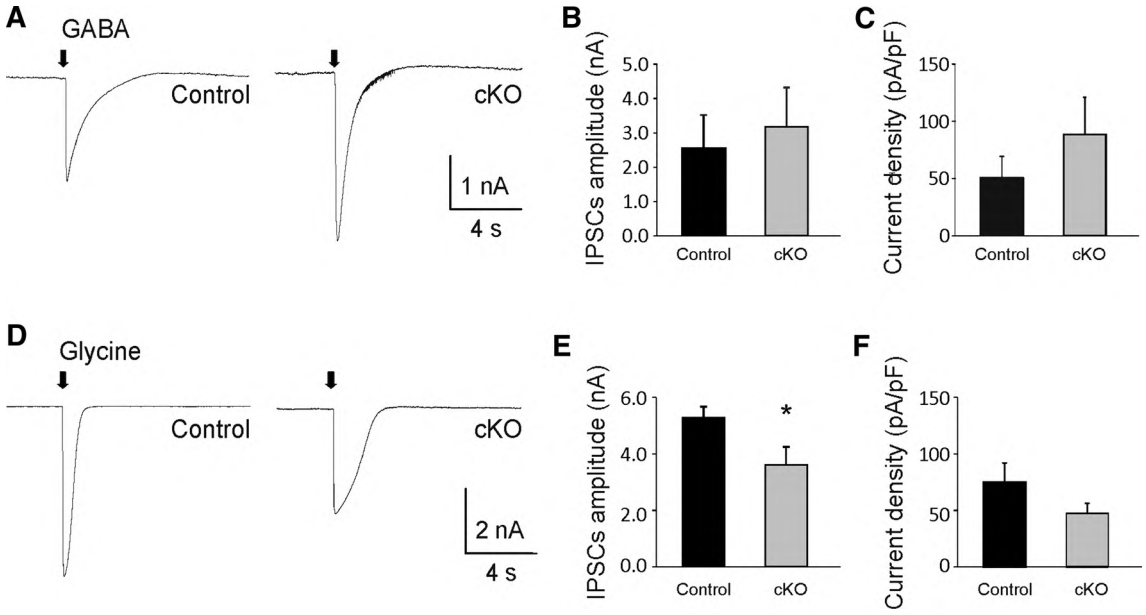

Fig. 8 Evoked postsynaptic glycinergic currents (eIPSCs) are reduced in hypoglossal neurons of *VIAAT* cKO embryos. **a** Averaged GABAergic eIPSC recorded from hypoglossal neurons of Ctrl and cKO embryos. *Arrow* indicates puff-application of GABA (10 mM; ~1 bar, 20 ms). Action currents are truncated. **b**, **c** Basic statistical description of the amplitude (**b**) and current density (**c**) of GABAergic eIPSCs. **d** Averaged glycinergic evoked IPSC. *Arrow* indicates puff-application of glycine (1 mM; 1 bar, 20 ms). **e** the average amplitude of glycinergic eIPSC was significantly smaller in cKO embryos as compared to Ctrl embryos. **f** Changes of current density are however not signifcant; *Bar graphs* mean ± SEM

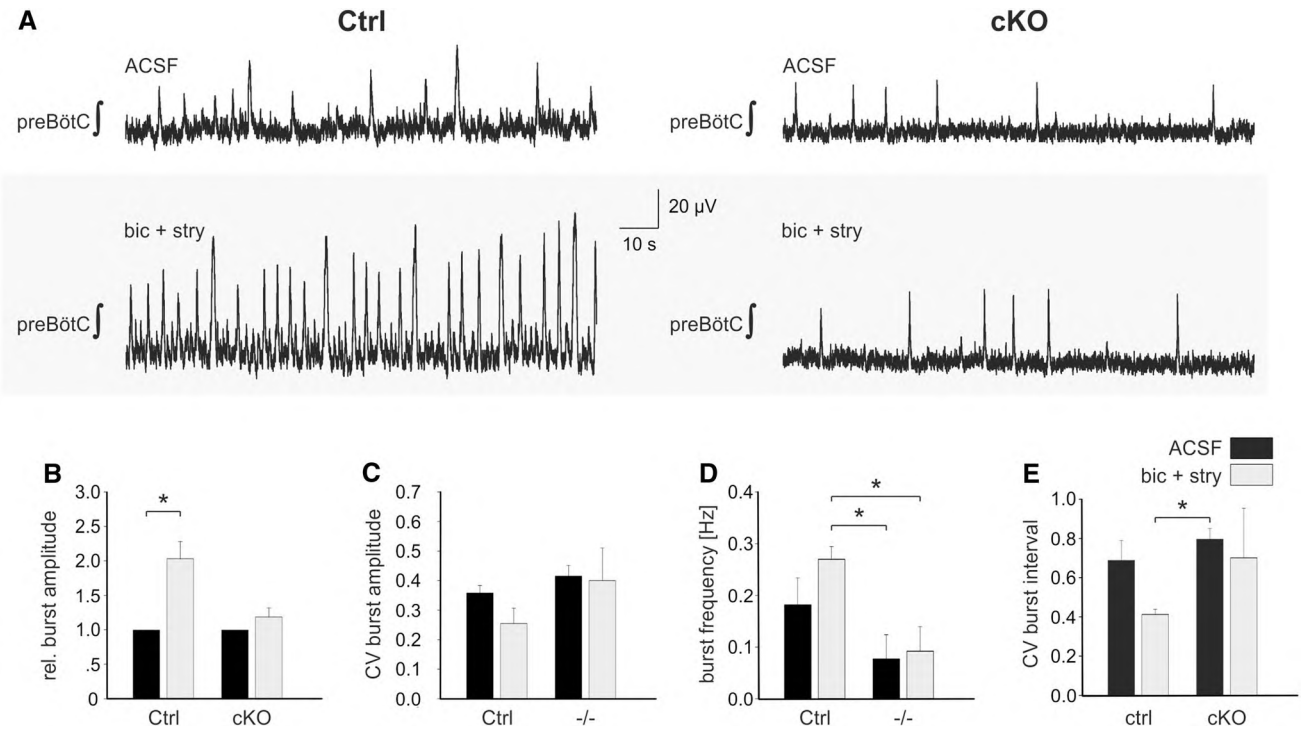

Fig. 9 Analysis of respiratory rhythmic slices from *VIAAT* cKO and Ctrl mice. **a** Field potential recordings from the preBötzinger Complex (preBötC) in control solution (ACSF) and after complete blockade of synaptic inhibition by bicuculline (bic 20 µM) and strychnine (stry 10 µM). **b**-**e** basic statistical discription of experiments. Respiratory rhythmic activity can be recorded in both Ctrl and *VIAAT* cKO mice; however, the activity in the cKO slices tended to be weaker. Furthermore, only Ctrl slices responded to blockade of inhibitory transmitter receptors with an increase of the burst amplitude (**b**) and frequency (n.s.; **d**). *Bar graphs* mean ± SEM

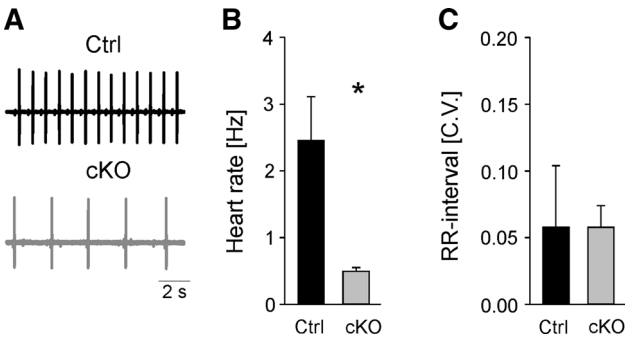

Fig. 10 Bradycardia is evident in *VIAAT* cKO embryos. **a** Electrocardiogram (ECG) from a Ctrl embryo and from a *VIAAT* cKO littermate (KO). **b** Basic statistics of heart rate and **c** heart rate variability (*C.V.* coefficient of variation)

inhibitory neurons by 10 μM strychnine and 20 μM bicuculline alters network activity. In Ctrl mice the preBötC activity indeed increased significantly, while there was no effect observed in the cKO mice (Fig. 9). Especially, the burst amplitude was increased by a factor of 2 in WT slices. Again, these data suggest that synaptic inhibition is abolished in the brainstem of *VIAAT* cKO embryos. However, we can assume that a basal network activity that is based on excitatory neurons can be generated in the preBötzinger complex of cKO embryos.

Autonomic effects in *VIAAT* cKOs

The strong reduction of VIAAT expression detected in the ventrolateral medulla and the loss of inhibition in the preBötC suggests that, in addition to the loss of inhibition affecting respiratory neurons, neighboring inhibitory cardiac interneurons have also lost VIAAT resulting in a reduction of inhibition of parasympathetic preganglionic cardiac vagal neurons in the nucleus ambiguus and bradycardia (Bentzen and Grunnet 2011). To test this hypothesis, we measured embryonic heart rates (HR) using ECG. Indeed, the HR of *VIAAT* cKO mice was significantly reduced (Fig. 10). In Ctrl mice, HR was 2.45 ± 1.47 Hz ($n = 5$) while it was only 0.50 ± 0.11 Hz in cKOs ($n = 4$; $p < 0.05$; Mann–Whitney Rank Sum Test), indicating that autonomic regulation was also impaired in *VIAAT* cKOs.

Discussion

We found that a neuron-type specific conditional deletion of *VIAAT* in glycinergic neurons produces a phenocopy of *VIAAT* KOs with a global deletion of the gene (Saito et al. 2010; Fujii et al. 2007; Wojcik et al. 2006; Oh et al. 2010), although significant inactivation of the *VIAAT* gene only occurred in caudal regions of the CNS. The severe disturbance of both glycinergic and GABAergic synaptic inhibition in brainstem results in a lethal disturbance of the cardio-respiratory network.

Implications for glycinergic synaptic inhibition

Our data provide important information for understanding the complex development of synaptic inhibition in the brainstem. Glycinergic transmission is eliminated in the *VIAAT* cKO mice, which supports the concept that VIAAT is the only vesicular transporter for glycine in the brainstem (Wojcik et al. 2006). The absence of any significant residual glycine release in the *VIAAT* cKO furthermore implies that the residual synaptic glycine release (Latal et al. 2010) observed in *GlyT2* KO mice (Gomeza et al. 2003b) results from alternative glycine supply routes to the presynaptic terminal such as reverse operation of the glycine cleavage system (Beyoglu and Idle 2012; Kikuchi 1973) or low affinity transporters like ASC-1 (Nakauchi et al. 2000) or SNAT2 (Yao et al. 2000). Such alternative supply routes should thus be considered when interpreting data from *GlyT2* KO mice that have an isolated failure of glycinergic transmission, but usually survive until the second postnatal week (Gomeza et al. 2003b) although GABA transmission was not up-regulated in *GlyT2* KO mice (Latal et al. 2010). Similarly, in *VIAAT* cKO mice, we found no evidence for a compensatory up-regulation of either transmitter system; neither on the pre- nor on the postsynaptic site.

GABA/glycine co-transmission in the embryonic hindbrain

Expression of GlyT2 starts at E11 (Zafra et al. 1995b) and is fully developed and restricted to the hindbrain at E18 (Zafra et al. 1995a; Jursky and Nelson 1996). The fact that in the brainstem of *GlyT2-Cre VIAAT* cKO mice, not only glycinergic but also GABAergic transmission is absent suggests that most glycinergic neurons, at least temporarily, also release GABA. Thus it appears that co-transmission is abundant in the caudal CNS during embryonic development. Indeed, our analysis of GABA-immunoreactivity in the embryonic hindbrain (at E15.5 and E17.5) revealed that less than 15 % of inhibitory neurons were purely GABAergic while 65 % where cotransmitting. After birth, however, co-transmission appears to become less relevant and the percentage of cotransmitting neurons drops to about 40 % (Fig. 6). This matches earlier single cell PCR data from our group where approximately 40 % of the glycinergic neurons in the preBötC of newborn mice were found to express a GABAergic marker protein

(GAD65, GAD67, or GAT1; Rahman et al. 2013). Thus, during the first 1–2 postnatal weeks that *GlyT2* KO mice usually survive (Gomeza et al. 2003a; Latal et al. 2010) the high overlap of the two inhibitory neuron populations might, at least temporarily, help to rescue inhibitory connections in the cardio-respiratory network in mouse lines that have defects in only one transmitter system.

Restriction of *VIAAT* cKO to caudal brain regions

In *VIAAT* cKO embryos the reduction of *VIAAT* expression was restricted to the hindbrain, as we did not observe changes in ventromedial hypothalamus (Fig. 5). The lack of recombination in rostral brain regions in *VIAAT* cKO mice suggests that the cortex and midbrain staining previously observed in adult *GlyT2-Cre*/ROSA26/LacZ reporter double transgenic mice (Ishihara et al. 2010), is indicative of accumulation of Cre recombinase activity over time rather than of significant expression of *GlyT2-Cre* in the embryonic forebrain. Moreover, our data clearly show that the phenotype of the conventional *VIAAT* KO is determined by the hindbrain pathology.

Developmental aspects of the *VIAAT* cKO phenotype

While cardio-respiratory failure appears to be the primary cause of death, the persistence of the embryonic umbilical hernia or omphalocele can have a negative effect on the detection of stillborn *VIAAT* cKO pups delivered naturally, since dams tend to eat stillborn mice with gut herniation very quickly (Shimizu et al. 2005; Turgeon and Meloche 2009). The loss of GABAergic transmission is apparently a major factor in the failure to retract the umbilical hernia or the defective closure of the abdominal wall, since *GAD67* KO mice also show an umbilical hernia/omphalocele, although with only 85 % penetrance (Oh et al. 2010). Closure of the abdominal wall occurs between E15.5 and E16.5 (Shimizu et al. 2005), at precisely the time when the chloride equilibrium potential $E_{[Cl]}^{-}$ in spinal motoneurons falls below the threshold for action potentials and GABAergic postsynaptic potentials, although depolarizing, will produce shunting inhibition (Delpy et al. 2008). Consistent with the idea that synaptic inhibition appears to be crucial for the repositioning of the gut to the peritoneal cavity and/or for the proper closure of the body wall, omphalocele also occurs in *KCC2* KO mice, where chloride-mediated inhibition remains excitatory (Hubner et al. 2001) and in *Neurobeachin* KOs, where synaptic release of GABA and glycine is almost absent (Medrihan et al. 2009).

The lack of GABAergic transmission to the hypoglossal nerve has also been implicated in the failure of palate closure in *VIAAT* KO mice (Saito et al. 2010) that is also observed in *GAD67* KO mice (Condie et al. 1997) and *Gabrb3* KOs (Ferguson et al. 2007). Embryonic tongue movements are strongly reduced in *GAD67* KO E14 fetuses or after $GABA_AR$ blockade (Tsunekawa et al. 2005), which may interfere with palate closure. However, GABA itself may be required for palate closure, as blockade of $GABA_A$ receptors can induce cleft palate (Ding et al. 2004) and activation of $GABA_A$ receptors by muscimol can rescue it (Oh et al. 2010). Interestingly, a cleft palate is not observed in *KCC2* KOs (Hubner et al. 2001), which suggests that the cleft palate results from a lack of the excitatory effects of GABA before E15.5, i.e. the time point when significant KCC2 expression is observed in the relevant brain areas.

Failure of breathing in *VIAAT* cKO mice

In the preBötC, spontaneous activity is mediated by a network of excitatory pacemaker neurons (Butera et al. 1999; Wallen-Mackenzie et al. 2006), whose functional integrity is a prerequisite for breathing (Gray et al. 2001). In WT E18.5 embryos the activity increases after application of strychnine and bicuculline, which is in line with the concept that glycinergic and GABAergic neurons are integrated in the early respiratory network (Winter et al. 2009; Morgado-Valle et al. 2010; Kuwana et al. 2006) and that their transmission is inhibitory at birth (Gomeza et al. 2003a). In the preBötC of *VIAAT* cKO embryos basal burst activity could still be recorded, while its modulation by strychnine and bicuculline was completely lost. However, the low frequency of preBötC activity is rather surprising and suggests that the loss of synaptic release of inhibitory transmitters has an additional developmental effect on the preBötC network. This observation is in line with data from brainstem spinal cord en-bloc preparations of *VIAAT* KOs, showing lack of phrenic (C4) output, while neurons in the rostral ventrolateral medulla are still spontaneously active (Fujii et al. 2007). Our analysis of *VIAAT* cKO adds to the notion that respiratory neurons are basically healthy, but network interactions in the preBötC are disturbed. At E18.5 the central respiratory rhythm generator consists of two coupled oscillators, the rostral para-facial respiratory group (pFRG), at the level of the cranial nerve VII, and the preBötC in the ventrolateral medulla (Thoby-Brisson et al. 2009). While both oscillators contain excitatory pacemaker neurons (Janczewski et al. 2002; Butera et al. 1999) their interaction by inhibitory feedback from the preBötC to the pFRG is important for normal respiratory activity (Onimaru et al. 1990; Lal et al. 2011; Wittmeier et al. 2008). It is interesting to note that network activity in *GAD65/GAD67* double KO embryos, which lack only the GABAergic part of inhibitory transmission, can be rescued by application of Substance P (Fujii et al. 2007), while in *VIAAT* KO mice, Substance P is unable to induce any C4 activity (Fujii et al. 2007). Later experiments demonstrate

that both transmitters systems, glycine and GABA, are involved in the function of the respiratory network and temporary postnatal survival of mice with loss of only one transmitter system might therefore be due to the fact that inhibitory respiratory neurons co-release glycine and GABA.

Conclusion

Our data demonstrate that the development and function of the respiratory network around birth depend on intact inhibitory synaptic transmission. Furthermore, since not only glycinergic, but also GABAergic transmission is virtually absent in the brainstem of *GlyT2-Cre* driven *VIAAT* cKO mice, a large overlap of glycinergic and GABAergic neurons during fetal development is evident. Taken together, our data strongly support the idea of a significant developmental overlap between the GABAergic and glycinergic neuronal populations in the embryonic hindbrain, with GABA/glycine co-transmission as the dominant mode of synaptic transmission.

Acknowledgments This work was funded by the Cluster of Excellence and DFG Research Center Nanoscale Microscopy and Molecular Physiology of the Brain (CNMPB). SH and JH received additional support from the DFG (Hu797/7-1, 8-1; Hi1414/2-1). The authors are grateful to Anja-Annett Grützner, Astrid Zeuch, Astrid Ohle and Annette Fahrenholz for technical assistance.

References

Aubrey KR, Rossi FM, Ruivo R, Alboni S, Bellenchi GC, Le Goff A, Gasnier B, Supplisson S (2007) The transporters GlyT2 and VIAAT cooperate to determine the vesicular glycinergic phenotype. J Neurosci 27(23):6273–6281. doi:10.1523/JNEUROSCI.1024-07.2007

Bentzen BH, Grunnet M (2011) Central and peripheral GABA(A) receptor regulation of the heart rate depends on the conscious state of the animal. Adv Pharmacol Sci 2011:578273. doi:10.1155/2011/578273

Beyoglu D, Idle JR (2012) The glycine deportation system and its pharmacological consequences. Pharmacol Ther 135(2): 151–167. doi:10.1016/j.pharmthera.2012.05.003

Butera RJ Jr, Rinzel J, Smith JC (1999) Models of respiratory rhythm generation in the pre-Botzinger complex. I. Bursting pacemaker neurons. J Neurophysiol 82(1):382–397

Condie BG, Bain G, Gottlieb DI, Capecchi MR (1997) Cleft palate in mice with a targeted mutation in the gamma-aminobutyric acid-producing enzyme glutamic acid decarboxylase 67. Proc Natl Acad Sci USA 94(21):11451–11455

Davies LP, Johnston GA (1974) Postnatal changes in the levels of glycine and the activities of serine hydroxymethyltransferase and glycine:2-oxoglutarate aminotransferase in the rat central nervous system. J Neurochem 22(1):107–112

Delpy A, Allain AE, Meyrand P, Branchereau P (2008) NKCC1 cotransporter inactivation underlies embryonic development of chloride-mediated inhibition in mouse spinal motoneuron. J Physiol 586(4):1059–1075. doi:10.1113/jphysiol.2007.146993

Ding R, Tsunekawa N, Obata K (2004) Cleft palate by picrotoxin or 3-MP and palatal shelf elevation in GABA-deficient mice. Neurotoxicol Teratol 26(4):587–592. doi:10.1016/j.ntt.2004.04.002

Drorbaugh JE, Fenn WO (1955) A barometric method for measuring ventilation in newborn infants. Pediatrics 16(1):81–87

Feng G, Tintrup H, Kirsch J, Nichol MC, Kuhse J, Betz H, Sanes JR (1998) Dual requirement for gephyrin in glycine receptor clustering and molybdoenzyme activity. Science 282(5392): 1321–1324

Ferguson C, Hardy S, Werner D, Hileman S, DeLorey T, Homanics G (2007) New insight into the role of the beta3 subunit of the GABAA-R in development, behavior, body weight regulation, and anesthesia revealed by conditional gene knockout. BMC Neurosci 8(1):85

Fujii M, Arata A, Kanbara-Kume N, Saito K, Yanagawa Y, Obata K (2007) Respiratory activity in brainstem of fetal mice lacking glutamate decarboxylase 65/67 and vesicular GABA transporter. Neuroscience 146(3):1044–1052. doi:10.1016/j.neuroscience.2007.02.050

Gomeza J, Hulsmann S, Ohno K, Eulenburg V, Szoke K, Richter D, Betz H (2003a) Inactivation of the glycine transporter 1 gene discloses vital role of glial glycine uptake in glycinergic inhibition. Neuron 40(4):785–796

Gomeza J, Ohno K, Hulsmann S, Armsen W, Eulenburg V, Richter DW, Laube B, Betz H (2003b) Deletion of the mouse glycine transporter 2 results in a hyperekplexia phenotype and postnatal lethality. Neuron 40(4):797–806

Gray PA, Janczewski WA, Mellen N, McCrimmon DR, Feldman JL (2001) Normal breathing requires preBotzinger complex neurokinin-1 receptor-expressing neurons. Nat Neurosci 4(9):927–930. doi:10.1038/nn0901-927

Gunther U, Benson J, Benke D, Fritschy JM, Reyes G, Knoflach F, Crestani F, Aguzzi A, Arigoni M, Lang Y et al (1995) Benzodiazepine-insensitive mice generated by targeted disruption of the gamma 2 subunit gene of gamma-aminobutyric acid type A receptors. Proc Natl Acad Sci USA 92(17):7749–7753

Hubner CA, Stein V, Hermans-Borgmeyer I, Meyer T, Ballanyi K, Jentsch TJ (2001) Disruption of KCC2 reveals an essential role of K–Cl cotransport already in early synaptic inhibition. Neuron 30(2):515–524

Hulsmann S, Oku Y, Zhang W, Richter DW (2000) Metabotropic glutamate receptors and blockade of glial Krebs cycle depress glycinergic synaptic currents of mouse hypoglossal motoneurons. Eur J Neurosci 12(1):239–246

Ishihara N, Armsen W, Papadopoulos T, Betz H, Eulenburg V (2010) Generation of a mouse line expressing Cre recombinase in glycinergic interneurons. Genesis 48(7):437–445. doi:10.1002/dvg.20640

Janczewski WA, Onimaru H, Homma I, Feldman JL (2002) Opioid-resistant respiratory pathway from the preinspiratory neurones to abdominal muscles: in vivo and in vitro study in the newborn rat. J Physiol 545(Pt 3):1017–1026. doi:10.1113/jphysiol.2002.023408

Jo YH (2012) Endogenous BDNF regulates inhibitory synaptic transmission in the ventromedial nucleus of the hypothalamus. J Neurophysiol 107(1):42–49. doi:10.1152/jn.00353.2011

Jursky F, Nelson N (1995) Localization of glycine neurotransmitter transporter (GLYT2) reveals correlation with the distribution of glycine receptor. J Neurochem 64(3):1026–1033. doi:10.1046/j.1471-4159.1995.64031026.x

Jursky F, Nelson N (1996) Developmental expression of the glycine transporters GLYT1 and GLYT2 in mouse brain. J Neurochem 67(1):336–344

Kikuchi G (1973) The glycine cleavage system: composition, reaction mechanism, and physiological significance. Mol Cell Biochem 1(2):169–187. doi:10.1007/BF01659328

Kling C, Koch M, Saul B, Becker CM (1997) The frameshift mutation oscillator [Glra1(spd-ot)] produces a complete loss of glycine receptor alpha1-polypeptide in mouse central nervous system. Neuroscience 78(2):411–417

Kuwana S, Tsunekawa N, Yanagawa Y, Okada Y, Kuribayashi J, Obata K (2006) Electrophysiological and morphological characteristics of GABAergic respiratory neurons in the mouse pre-Botzinger complex. Eur J Neurosci 23(3):667–674. doi:10.1111/j.1460-9568.2006.04591.x

Lal A, Oku Y, Hulsmann S, Okada Y, Miwakeichi F, Kawai S, Tamura Y, Ishiguro M (2011) Dual oscillator model of the respiratory neuronal network generating quantal slowing of respiratory rhythm. J Comput Neurosci 30(2):225–240. doi:10.1007/s10827-010-0249-0

Latal AT, Kremer T, Gomeza J, Eulenburg V, Hulsmann S (2010) Development of synaptic inhibition in glycine transporter 2 deficient mice. Mol Cell Neurosci 44(4):342–352. doi:10.1016/j.mcn.2010.04.005

Liu P, Jenkins NA, Copeland NG (2003) A highly efficient recombineering-based method for generating conditional knockout mutations. Genome Res 13(3):476–484

Luque JM, Nelson N, Richards JG (1995) Cellular expression of glycine transporter 2 messenger RNA exclusively in rat hindbrain and spinal cord. Neuroscience 64(2):525–535. doi:10.1016/0306-4522(94)00404-S

McIntire SL, Reimer RJ, Schuske K, Edwards RH, Jorgensen EM (1997) Identification and characterization of the vesicular GABA transporter. Nature 389(6653):870–876. doi:10.1038/39908

Medrihan L, Rohlmann A, Fairless R, Andrae J, Doring M, Missler M, Zhang W, Kilimann MW (2009) Neurobeachin, a protein implicated in membrane protein traffic and autism, is required for the formation and functioning of central synapses. J Physiol 587(Pt 21):5095–5106. doi:10.1113/jphysiol.2009.178236

Morgado-Valle C, Baca SM, Feldman JL (2010) Glycinergic pacemaker neurons in preBotzinger complex of neonatal mouse. J Neurosci 30(10):3634–3639. doi:10.1523/JNEUROSCI.3040-09.2010

Nakauchi J, Matsuo H, Kim DK, Goto A, Chairoungdua A, Cha SH, Inatomi J, Shiokawa Y, Yamaguchi K, Saito I, Endou H, Kanai Y (2000) Cloning and characterization of a human brain Na+-independent transporter for small neutral amino acids that transports D-serine with high affinity. Neurosci Lett 287(3):231–235. doi:10.1016/s0304-3940(00)01169-1

Oh WJ, Westmoreland JJ, Summers R, Condie BG (2010) Cleft palate is caused by CNS dysfunction in Gad1 and VIAAT knockout mice. PLoS ONE 5(3):e9758. doi:10.1371/journal.pone.0009758

Onimaru H, Arata A, Homma I (1990) Inhibitory synaptic inputs to the respiratory rhythm generator in the medulla isolated from newborn rats. Pflug Arch 417(4):425–432

Paxinos G (2007) Atlas of the developing mouse brain: at E17.5, PO, and P6. Elsevier, Acad. Press, Amsterdam [u.a.]

Rahman J, Latal AT, Besser S, Hirrlinger J, Hulsmann S (2013) Mixed miniature postsynaptic currents resulting from co-release of glycine and GABA recorded from glycinergic neurons in the neonatal respiratory network. Eur J Neurosci 37(8):1229–1241. doi:10.1111/ejn.12136

Sagne C, El Mestikawy S, Isambert MF, Hamon M, Henry JP, Giros B, Gasnier B (1997) Cloning of a functional vesicular GABA and glycine transporter by screening of genome databases. FEBS Lett 417(2):177–183

Saito K, Kakizaki T, Hayashi R, Nishimaru H, Furukawa T, Nakazato Y, Takamori S, Ebihara S, Uematsu M, Mishina M, Miyazaki J, Yokoyama M, Konishi S, Inoue K, Fukuda A, Fukumoto M, Nakamura K, Obata K, Yanagawa Y (2010) The physiological roles of vesicular GABA transporter during embryonic development: a study using knockout mice. Mol Brain 3:40. doi:10.1186/1756-6606-3-40

Shimizu Y, Thumkeo D, Keel J, Ishizaki T, Oshima H, Oshima M, Noda Y, Matsumura F, Taketo MM, Narumiya S (2005) ROCK-I regulates closure of the eyelids and ventral body wall by inducing assembly of actomyosin bundles. J Cell Biol 168(6):941–953. doi:10.1083/jcb.200411179

Thoby-Brisson M, Karlen M, Wu N, Charnay P, Champagnat J, Fortin G (2009) Genetic identification of an embryonic parafacial oscillator coupling to the preBotzinger complex. Nat Neurosci 12(8):1028–1035. doi:10.1038/nn.2354

Tsunekawa N, Arata A, Obata K (2005) Development of spontaneous mouth/tongue movement and related neural activity, and their repression in fetal mice lacking glutamate decarboxylase 67. Eur J Neurosci 21(1):173–178. doi:10.1111/j.1460-9568.2004.03860.x

Turgeon B, Meloche S (2009) Interpreting neonatal lethal phenotypes in mouse mutants: insights into gene function and human diseases. Physiol Rev 89(1):1–26. doi:10.1152/physrev.00040.2007

Tyzio R, Cossart R, Khalilov I, Minlebaev M, Hubner CA, Represa A, Ben-Ari Y, Khazipov R (2006) Maternal oxytocin triggers a transient inhibitory switch in GABA signaling in the fetal brain during delivery. Science 314(5806):1788–1792. doi:10.1126/science.1133212

Wallen-Mackenzie A, Gezelius H, Thoby-Brisson M, Nygard A, Enjin A, Fujiyama F, Fortin G, Kullander K (2006) Vesicular glutamate transporter 2 is required for central respiratory rhythm generation but not for locomotor central pattern generation. J Neurosci 26(47):12294–12307. doi:10.1523/JNEUROSCI.3855-06.2006

Winter SM, Hirrlinger J, Kirchhoff F, Hulsmann S (2007) Transgenic expression of fluorescent proteins in respiratory neurons. Respir Physiol Neurobiol 159(1):108–114. doi:10.1016/j.resp.2007.05.009

Winter SM, Fresemann J, Schnell C, Oku Y, Hirrlinger J, Hulsmann S (2009) Glycinergic interneurons are functionally integrated into the inspiratory network of mouse medullary slices. Pflug Arch 458(3):459–469. doi:10.1007/s00424-009-0647-1

Wittmeier S, Song G, Duffin J, Poon CS (2008) Pacemakers handshake synchronization mechanism of mammalian respiratory rhythmogenesis. Proc Natl Acad Sci USA 105(46):18000–18005. doi:10.1073/pnas.0809377105

Wojcik SM, Katsurabayashi S, Guillemin I, Friauf E, Rosenmund C, Brose N, Rhee JS (2006) A shared vesicular carrier allows synaptic corelease of GABA and glycine. Neuron 50(4):575–587. doi:10.1016/j.neuron.2006.04.016

Yao D, Mackenzie B, Ming H, Varoqui H, Zhu H, Hediger MA, Erickson JD (2000) A novel system A isoform mediating Na+/neutral amino acid cotransport. J Biol Chem 275(30):22790–22797. doi:10.1074/jbc.M002965200

Zafra F, Aragon C, Olivares L, Danbolt NC, Gimenez C, Storm-Mathisen J (1995a) Glycine transporters are differentially expressed among CNS cells. J Neurosci 15(5 Pt 2):3952–3969

Zafra F, Gomeza J, Olivares L, Aragon C, Gimenez C (1995b) Regional distribution and developmental variation of the glycine transporters GLYT1 and GLYT2 in the rat CNS. Eur J Neurosci 7(6):1342–1352. doi:10.1111/j.1460-9568.1995.tb01125.x

Zeilhofer HU, Studler B, Arabadzisz D, Schweizer C, Ahmadi S, Layh B, Bosl MR, Fritschy JM (2005) Glycinergic neurons expressing enhanced green fluorescent protein in bacterial artificial chromosome transgenic mice. J Comp Neurol 482(2):123–141. doi:10.1002/cne.20349